Supporting Information

Bimetal synergistically regulates Ni and P oxidation states for efficient oxygen evolution reaction

Di Wang[a], Mengzhao Liu[a], Zhe Sun[a], Chaofan Zhang[a], Wenguang Cui[b], Chaozhen He[c], Zhongkui Zhao[a,*]

[a]*State Key Laboratory of Fine Chemicals, Department of Catalysis Chemistry and Engineering, School of Chemical Engineering, Dalian University of Technology, 2 Linggong Road, Dalian 116024, China*

[b]*College of Chemical Engineering Shijiazhuang University, 288 Zhufeng Street Shijiazhuang 050035, Hebei, China*

[c]*Institute of Environmental and Energy Catalysis, School of Materials Science and Chemical Engineering, Xi'an Technological University, Xi'an, 710021, China*

*Corresponding author：E-mail: zkzhao@dlut.edu.cn

Table of Contents

1. Experimental Section

Chemicals: Iron nitrate, red phosphorus and urea are all from Tianjin Damao Chemical Reagent Factory, KOH is from Aladdin, and manganese chloride is from Tianjin Guangfu Fine Chemical Research Institute.

Synthesis of Ni_2P: First, cut the foam nickel (NF) with a size of 1*1 cm^{-2}, put the NF into 2.0 M HCl solution and deionized water, respectively for 30 min ultrasonic, then put it into an oven for 10 h at 60 °C, and finally record the quality. 387 mg of red phosphorus (12.5 mmol) and 600 mg of urea (10 mmol) were dissolved in 10 ml of deionized water, stirred for 30 min, and then transferred to a hydrothermal kettle (volume: 40 ml, internal diameter: 27 mm, height: 70 mm). At the same time, the treated NF (4*1*1 cm^{-2}) was put into the kettle, and then the reaction was carried out at 190 °C for 24 h. After the reaction was cooled to room temperature, the catalyst was washed with deionized water, and the quality was recorded after being put into the oven for 10 h at 190 °C.

Synthesis of Ni_2P-ECO: A standard three-electrode system was used in the experiment. The dried Ni_2P was clamped on the electrode holder as the working electrode, the graphite rod as the opposite electrode, and Hg/HgO as the reference electrode. Electrooxidation reconstruction was performed for 30 minutes at 1.65 V (vs. RHE) with an electrolyte of 1.0 M KOH. The immersion area of the catalyst is 0.5 cm^{-2}.

Synthesis of (Fe)Ni_2P-ECO： A standard three-electrode system was used in the experiment. The dried Ni_2P was clamped on the electrode holder as the working electrode, the graphite rod as the opposite electrode, and Hg/HgO as the reference electrode. Electrooxidation reconstruction was performed for 30 minutes at 1.65 V (vs. RHE) with an electrolyte of 1.0 M KOH containing Fe^{3+} (10 μmol L^{-1}). The immersion area of the catalyst is 0.5 cm^{-2}.

Synthesis of (Mn)Ni_2P-ECO: A standard three-electrode system was used in the experiment. The dried Ni_2P was clamped on the electrode holder as the working electrode, the graphite rod as the opposite electrode, and Hg/HgO as the reference electrode. Electrooxidation reconstruction was performed for 30 minutes at 1.65 V (vs. RHE) with an electrolyte of 1.0 M KOH containing Mn^{3+} (10 μmol L^{-1}). The immersion area of the catalyst is 0.5 cm^{-2}.

Synthesis of (Fe,Mn)Ni_2P-ECO: A standard three-electrode system was used in the experiment. The dried Ni_2P was clamped on the electrode holder as the working electrode, the graphite rod as

the opposite electrode, and Hg/HgO as the reference electrode. Electrooxidation reconstruction was performed for 30 minutes at 1.65 V (vs. RHE) with an electrolyte of 1.0 M KOH containing Fe^{3+}/Mn^{2+}(mole ratio is 10:1). The immersion area of the catalyst is 0.5 cm^{-2}.

Characterization. Explore the morphology of the catalyst using the JEOL JSM-5600LV field emission scanning electron microscope (SEM). On a JEOL-2100F FETEM with an acceleration voltage of 80 kV, the intrinsic characteristics and element distribution of the catalyst were examined with transmission electron microscopy (TEM) and high-angle annular dark-field scanning transmission electron microscopy (HAADF-STEM). X-ray photoelectron spectroscopy (XPS) is a method of using the ESCALAB 250 XPS system with an Al Kα X-ray source (hv = 1486.6 eV). XRD was tested using the Rigaku Corporation SmartLab 9 X-ray diffractometer using Cu Kα radiation, scanning from 10° to 90° at a scanning speed of 3° per minute under voltage and current of 40 kV and 40 mA, respectively. The content of Fe and Mn was measured by an Optima 7300 DV inductively coupled plasma atomic emission spectrometer (ICP-AES).

Electrochemical measurements. The electrochemical test was evaluated by an electrochemical workstation (CHI 660E). A standard three-electrode system was used in the experiment, with a graphite rod as the counter electrode and Hg/HgO as the reference electrode. All data were calibrated with a standard hydrogen electrode (vs. RHE). The experiment was performed at room temperature with 85% infrared compensation (iR). For comparison, the linear sweep voltammetry (LSV) curves of all catalysts were scanned at 5 mV s^{-1} at a voltage of 1.03-1.73 V (vs. RHE), and the electrochemical impedance spectra were from 100 kHz to 0.01 Hz at an AC amplitude of 5 mV.

ECSA measurements. Electrochemical active surface area is calculated according to the Cdl, and cv curves can be obtained at different rates (20, 40, 60, 80, 100, 120, 140, 160 mV s -1) in 1.0-1.1 V (vs. RHE). ECSA is calculated as follows: ECSA (cm^{-2}) =Cdl/Cs; the value of Cs is 0.04 mF cm^{-2} and the ratio of the slope of the curve to the number of electrons transferred is Cdl.

TOF calculation. The density of active sites was measured by cyclic voltammetry in phosphate buffers with pH = 7 at a scanning rate of 50 mV s^{-1}.[25]Assuming that every atom is involved, the density of active sites n (mol g^{-1}) is directly proportional to the area of the cyclic voltammetry, calculated using the following formula: n = (5×A)/(F×m), where *A* is the effective area of the cyclic voltammetry curve after deducting the blank, *F* is Faraday's constant (96485.3C mol^{-1}), and

m is the catalyst mass on nickel foam. The TOF can be calculated using the following equation: TOF = j/(4×F×N), where *j* is the current density given by the LSV measurements, and *N* is the total number of active sites on the electrode calculated using the density of active sites *n* multiplied by the catalyst mass *m*.

FE% test. The test also adopted a three-electrode system with (Fe,Mn)Ni_2P-ECO (S = 0.5 cm^{-2}) as the working electrode. The whole electrolytic cell was purified with high-purity argon for about 30 minutes to reduce background interference. The volume of electrolytic liquid was 40 ml, and the volume of the upper cavity of the electrolytic cell was 74 ml. A chronopotentiometry test was performed at 5 mA for 2 h. The products were collected and analyzed in chromatography with high-purity argon (99.999%) as the carrier gas, equipped with a FID detector and a 5A molecular sieve-packed column. The Faraday efficiency of the product is calculated as follows:

$$FE\% = \frac{V \times \left[S_{Air2} \times S_{O_2} - S_{Air1} \times S_{N_2} + a \times S_{Air2}\right]}{b \times S_{Air2} \times 22.4 \times 298/273} \times \frac{96485 \times 4}{i \times t \times S} \times 100\%$$

S_{O_2}= the oxygen peak area after reaction-the initial oxygen peak area

S_{N_2}= the nitrogen peak area after reaction-the initial nitrogen peak area

S_{Air1}= the area of oxygen peak in the air

S_{Air2}= the area of nitrogen peak in the air

V: the volume of the cavity above the electrolytic cell

a: the intercept of the oxygen standard curve

b: the slope of the oxygen standard curve

i: electric current, A

t: electrolytic time, s.

S: catalyst area, cm^{-2}.

Computational details. Density functional theory (DFT) calculations were conducted using the Vienna ab initio simulation package (VASP).[18,19] The Generalized Gradient Approximation (GGA) with the Perdew-Burke-Ernzerhof (PBE) exchange-correlation functional was used for the exchange-correlation energy.[20] The projector augmented wave (PAW) method was used with a cutoff energy of 400 eV. Considering the Ni_2P (111) surface were found in our TEM image and

Ni_2P were transformed into NiOOH, a model of the Ni_2P (111) surface with a one-layer NiOOH was conducted. For the Ni_2P-NiOOH surface, 2 × 2 surface cells were built, with the bottom two layers of atoms fixed at their original bulk positions while the top two layers of atoms relaxed during geometric optimization. The dimension of the supercell is 13.52 Å × 13.52 Å × 15.53 Å with $\alpha = \beta = 90^\circ$, $\gamma = 97.58^\circ$, and a 10 Å vacuum slab was placed along the z axis on each slab to avoid the pseudo-interactions between periodic images. A Monkhorst-Pack grid of 2×2×1 size was used to sample the surface Brillouin zone.[20] The structures were optimized until the energies and forces on each atom were less than 1×10^{-5} eV and 0.03 eV $Å^{-1}$. According to previous studies, the DFT+U method was considered with U_{eff} = 5.5, 2.5, and 3.0 eV for Ni, Fe, and Mn, respectively. [22-24]

2. Supplementary Figures S1-S17 and Tables S1-S3

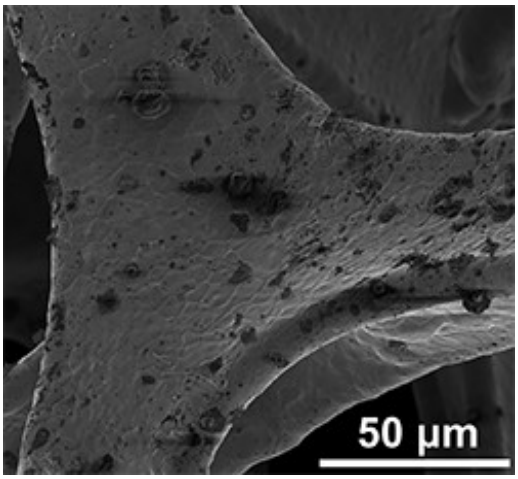

Figure S1. SEM image of NF with magnification.

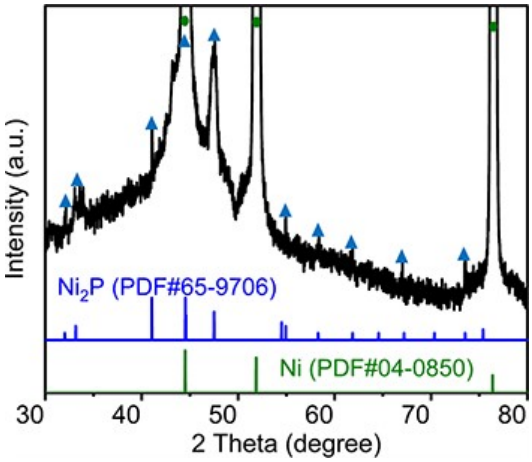

Figure S2. XRD pattern of Ni_2P.

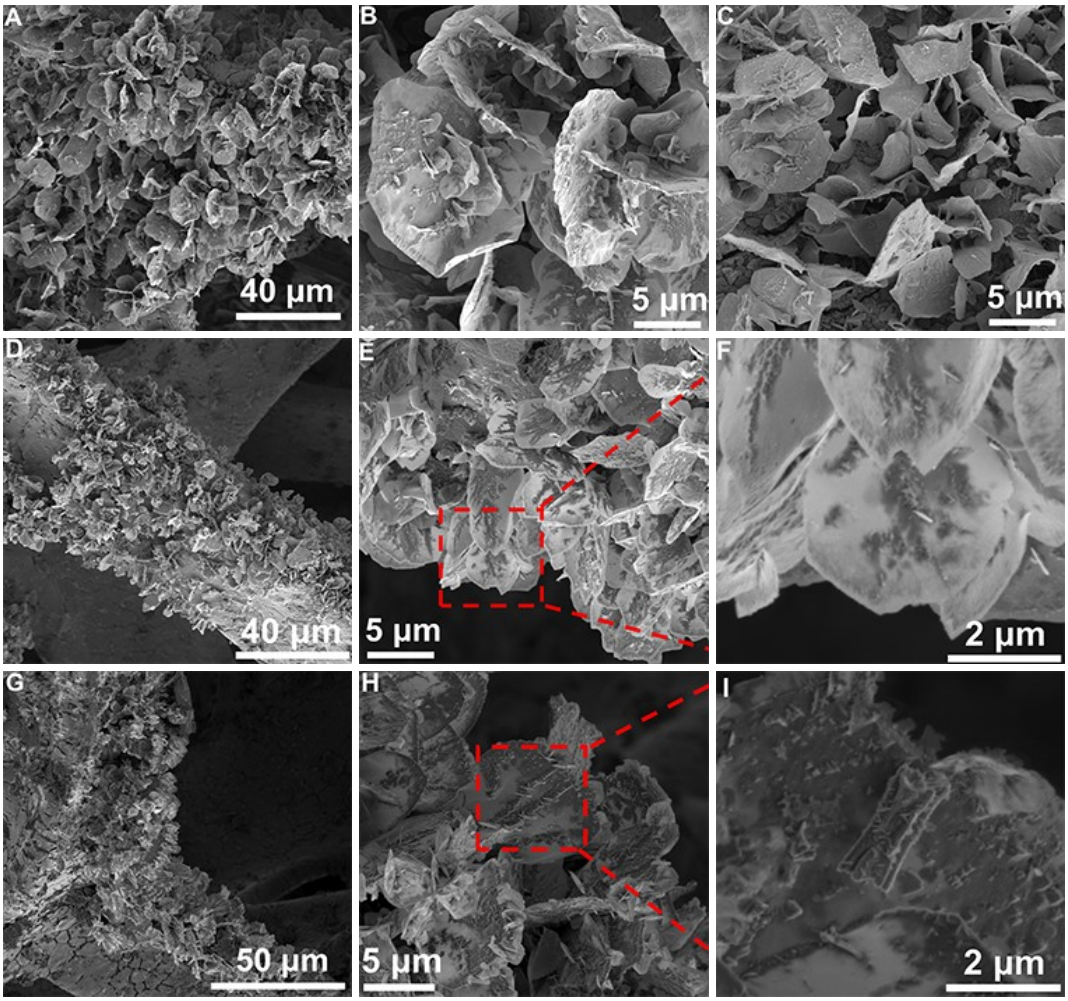

Figure S3. SEM images of (A and B) Ni_2P, (C) Ni_2P-ECO, (D-F) (Fe)Ni_2P-ECO, (G-I) (Mn)Ni_2P-ECO.

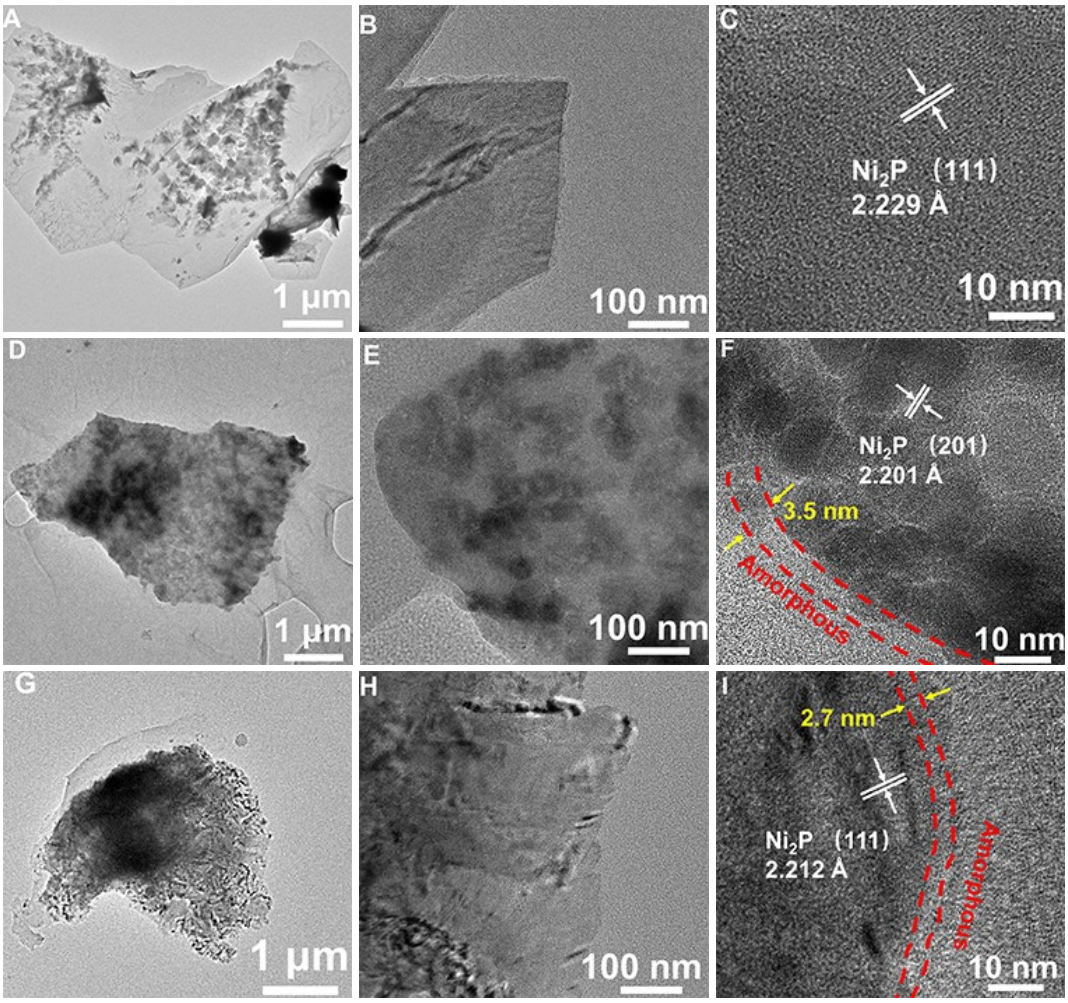

Figure S4. TEM images of (A-C) Ni_2P, (D-F) (Fe)Ni_2P-ECO, (G-I) (Mn)Ni_2P-ECO.

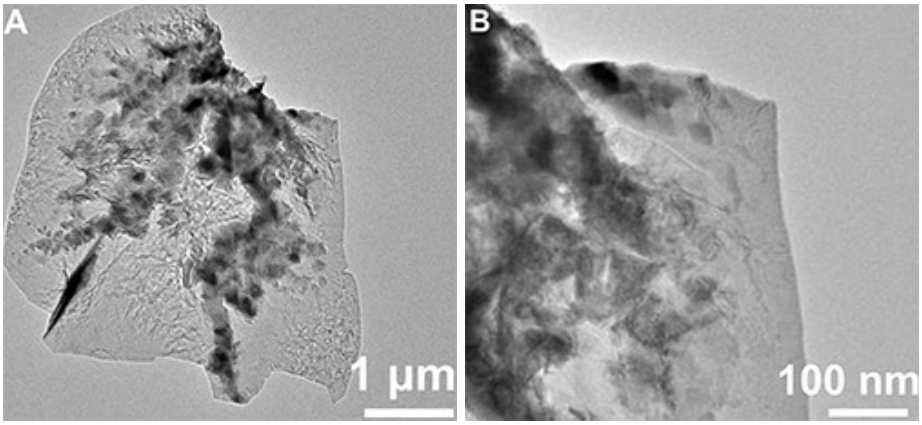

Figure S5. TEM images of Ni_2P-ECO.

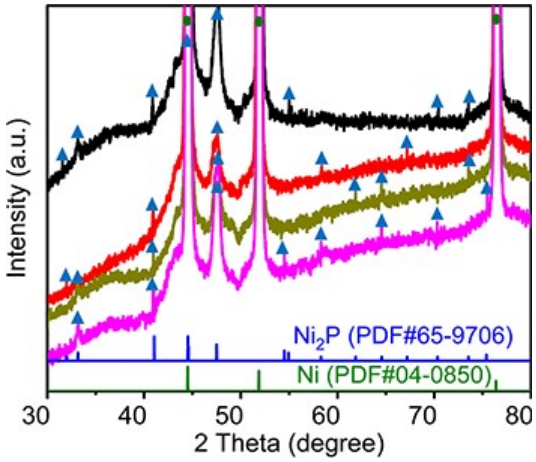

Figure S6. XRD pattern of catalysts. Color codes: black (Fe,Mn)Ni_2P-ECO, red (Fe)Ni_2P-ECO, dark yellow (Mn)Ni_2P-ECO and magenta Ni_2P-ECO.

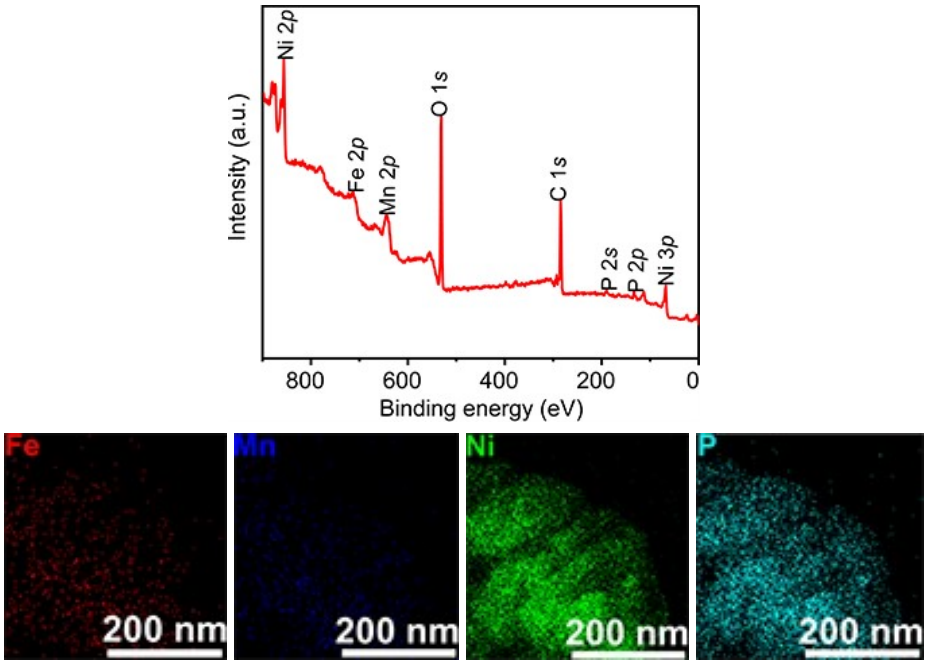

Figure S7. XPS survey spectrum of (Fe,Mn)Ni_2P-ECO and HAADF-STEM-EDS mapping of Fe, Mn, Ni and P for (Fe,Mn)Ni_2P-ECO.

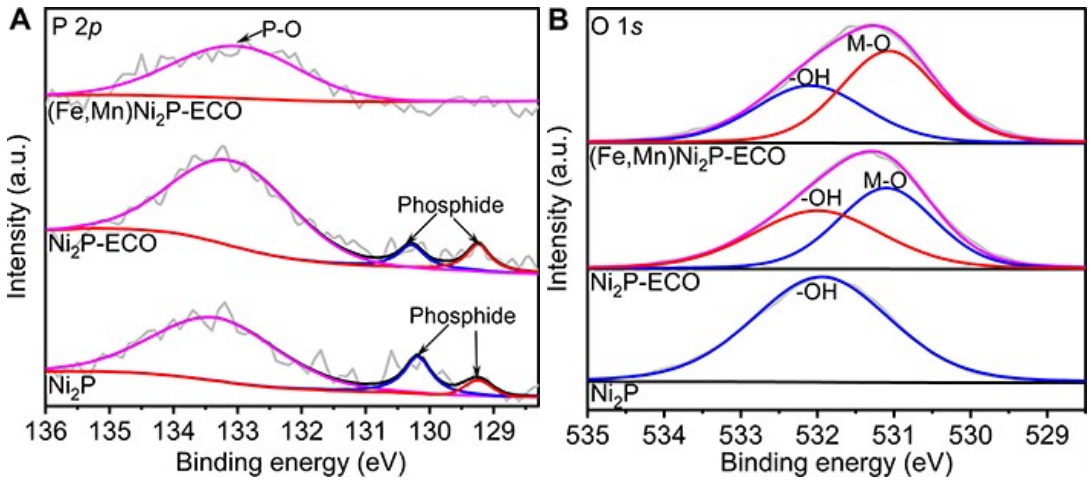

Figure S8. XPS spectra of (A) P 2*p* and (B) O 1*s*.

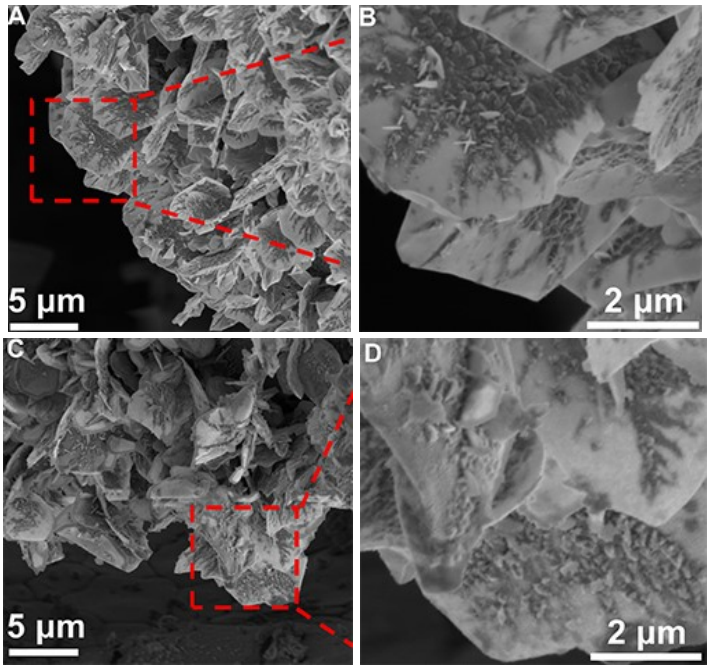

Figure S9. SEM images of (A and B) (Fe,Mn)Ni_2P-ECO , (C and D) (Fe,Mn)Ni_2P-ECO after OER for 100 h.

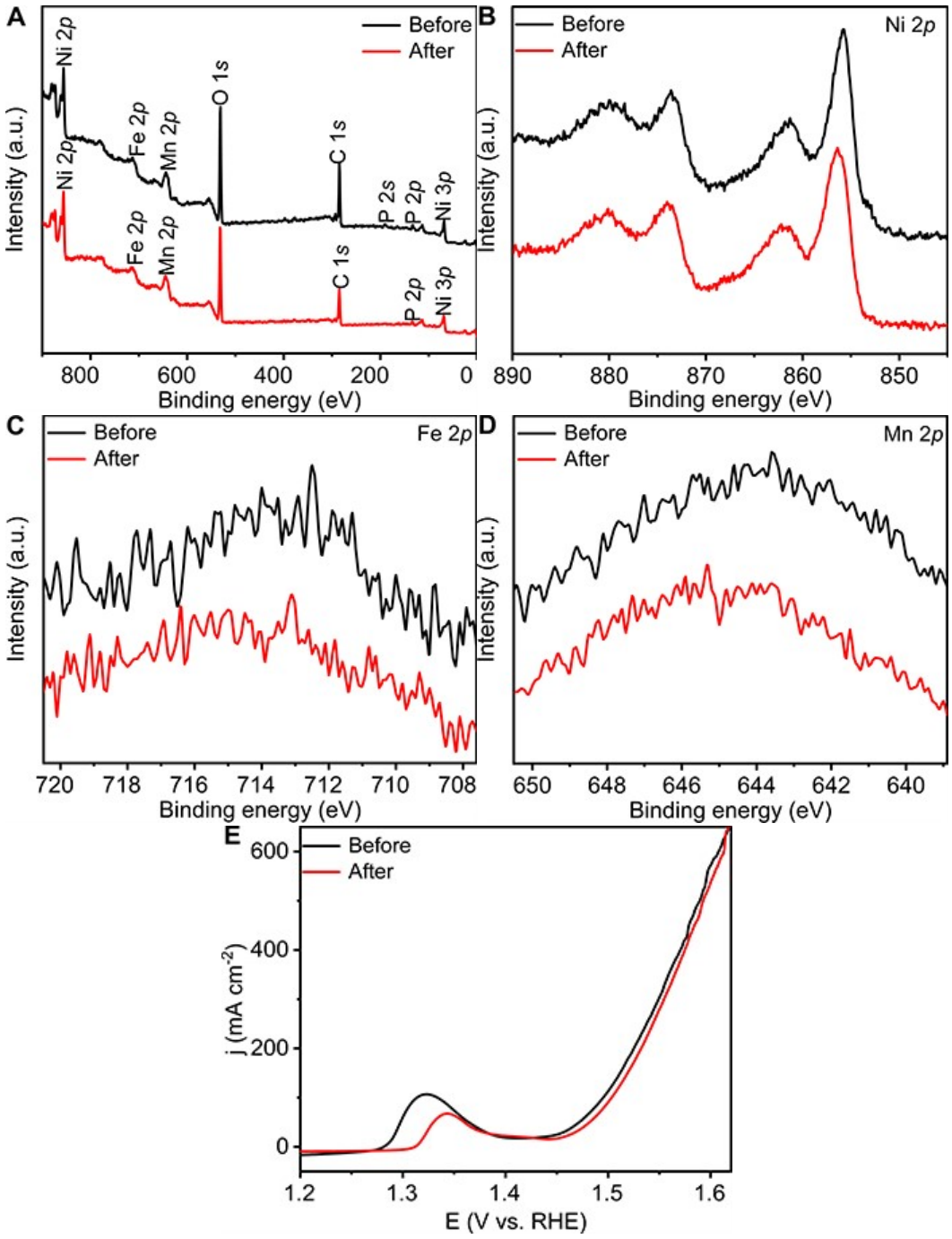

Figure S10. (A) XPS survey and (B-D) High-resolution XPS spectra: (B)Ni 2*p*, (C) Fe 2*p*, and (D) Mn 2p and (E) polarization curves in (Fe,Mn)Ni_2P-ECO before and after stability measurement.

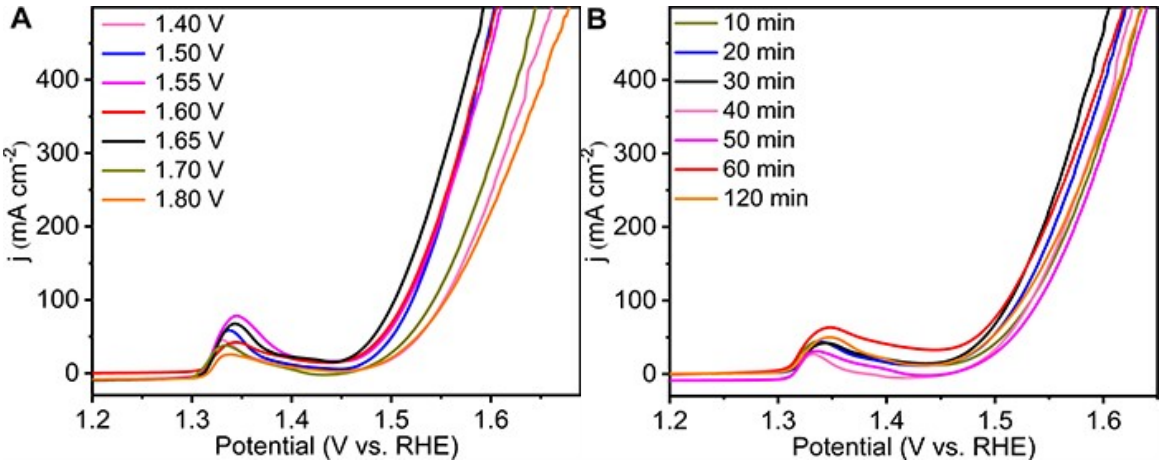

Figure S11. LSV curves for (Fe,Mn)Ni_2P-ECO of (A) different voltages at the same time 30 min, (B) different times at the same voltage 1.65 V (vs.RHE).

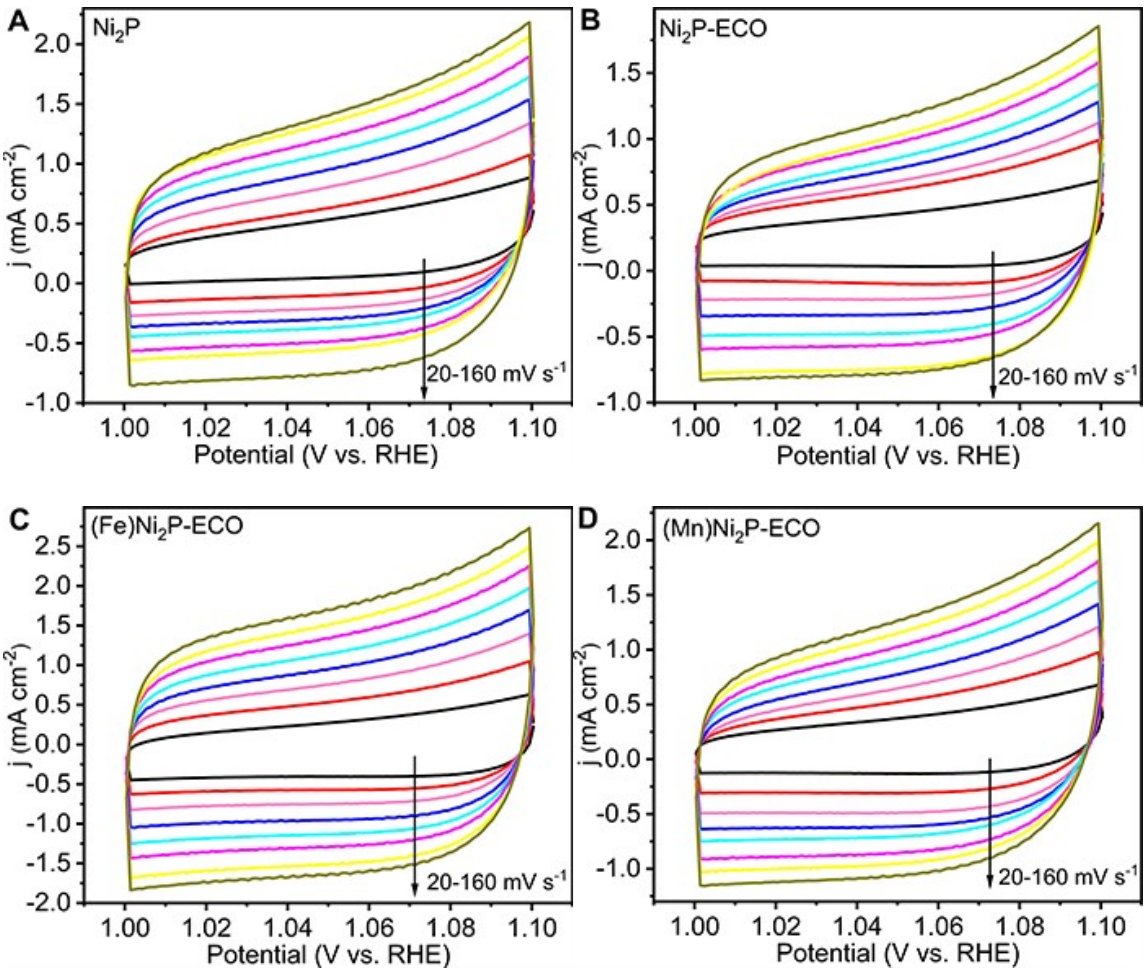

Figure S12. CV at various scan rates of 20, 40, 60, 80, 100, 120, 140 and 160 mV s^{-1} for (A) Ni_2P, (B) Ni_2P-ECO, (C) (Fe)Ni_2P-ECO and (D) (Mn)Ni_2P-ECO in 1.0 M KOH.

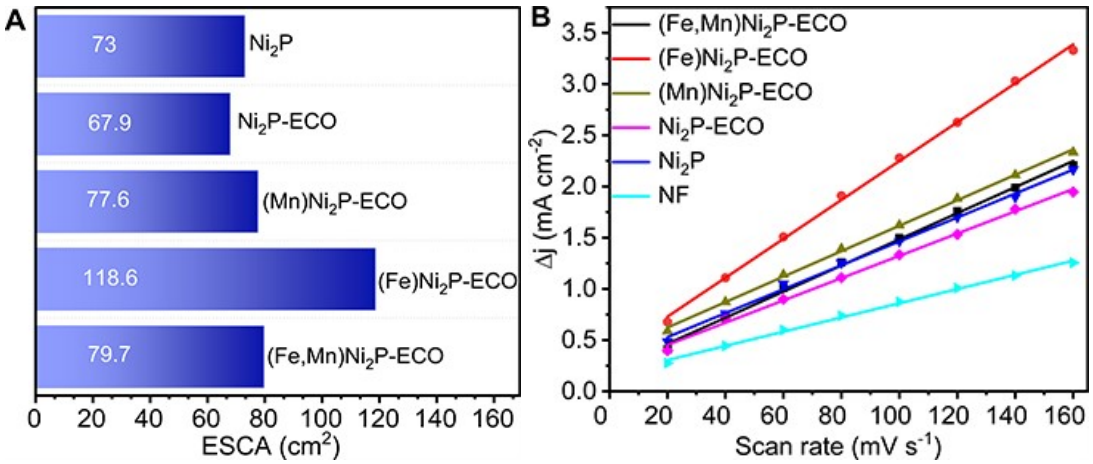

Figure S13. (A) ECSA and (B) double layer capacitance fitting curves of different catalysts in 1.0 M KOH.

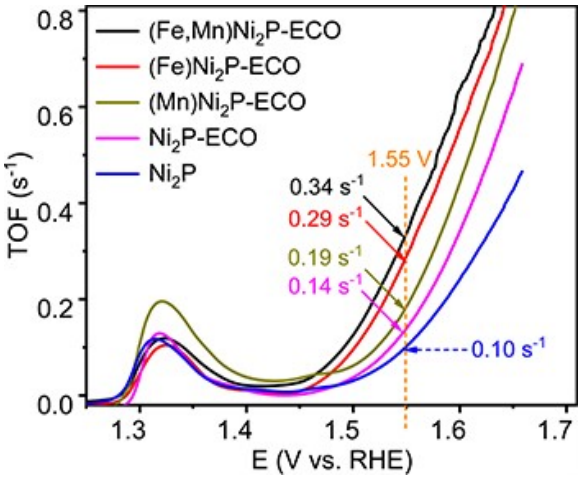

Figure S14. TOF curves of the Ni_2P, Ni_2P-ECO, (Fe)Ni_2P-ECO, (Mn)Ni_2P-ECO and (Fe,Mn)Ni_2P-ECO catalysts.

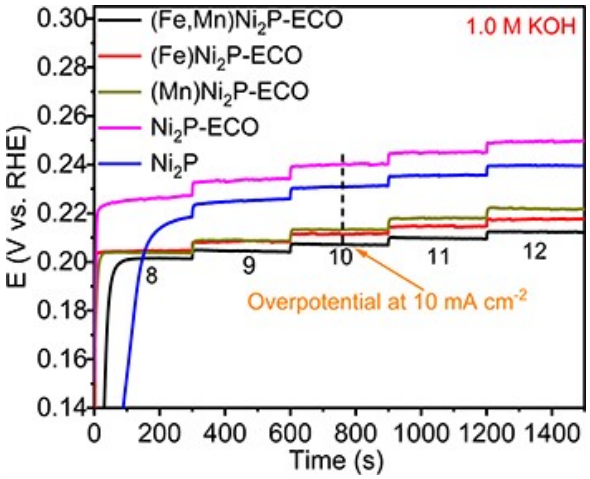

Figure S15. Chronopotentiometric plots of samples at different current densities in 1.0 M KOH.

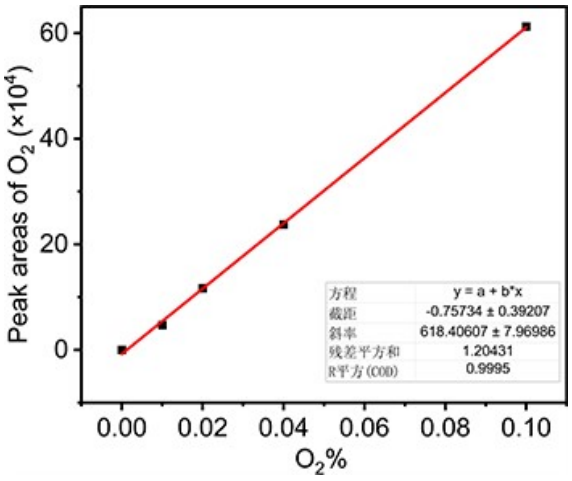

Figure S16. Standard graph of oxygen content.

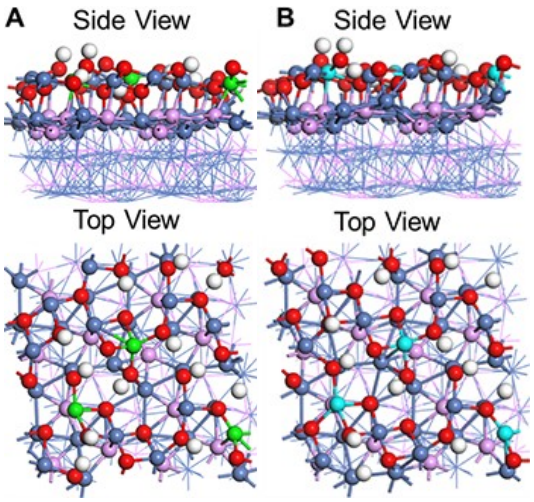

Figure S17. Structural models of (A) (Fe)Ni_2P-ECO catalyst (B) (Mn)Ni_2P-ECO catalyst. Color codes: green (Fe), cyan (Mn), blue (Ni), pink (P), red (O) and white (H).

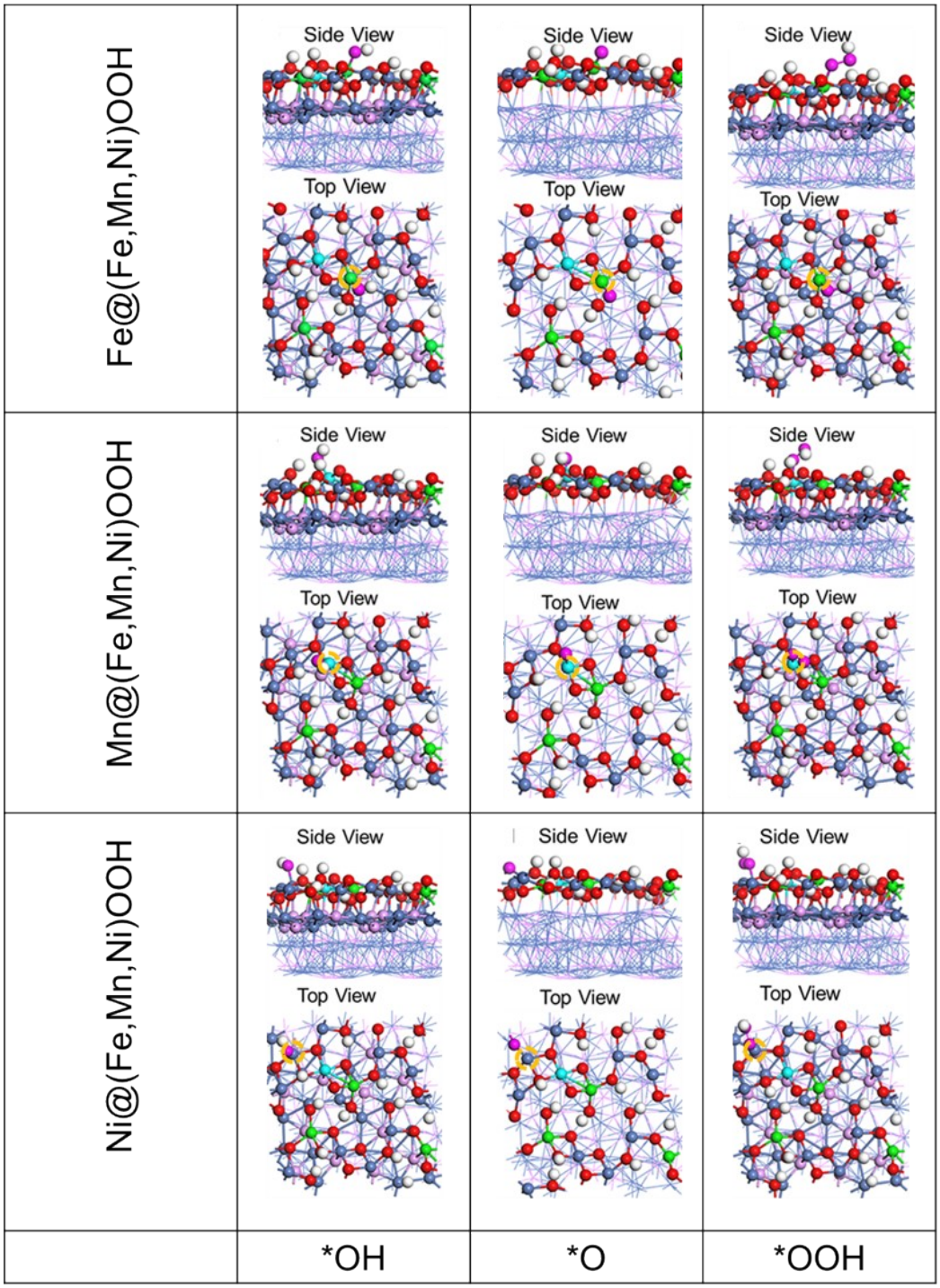

Figure S18. Optimized models for *O, *OH and *OOH intermediates of OER process on site of Fe@(Fe,Mn,Ni)OOH, Mn@(Fe,Mn,Ni)OOH, and Ni@(Fe,Mn,Ni)OOH. Color codes: green (Fe), cyan (Mn), blue (Ni), pink (P), white (H), red (oxygen of (Fe,Mn,Ni)OOH)) and magenta (oxygen of *OH, *O *OOH). The orange curve marks the best adsorption position.

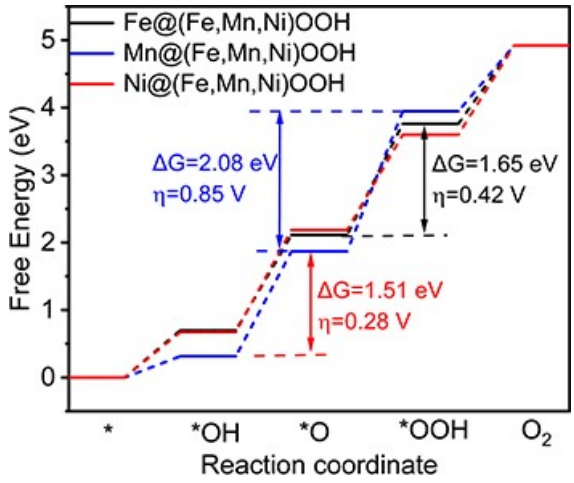

Figure S19. Gibbs free energy of different active adsorption sites for (Fe,Mn)Ni_2P-ECO catalyst.

Table S1. ICP-AES and EDX-mapping data for (Fe,Mn)Ni_2P-ECO.

Element	Mass% (ICP-AES)	Mass loading (mg cm^{-2})	Mass% (EDX-mapping)
Fe	0.36	0.98	0.62
Mn	0.00028	0.0078	0.01

Table S2. EDX-mapping data and the atomic content of M-OOH for (Fe,Mn)Ni_2P-ECO.

Element	Atom% (EDX-mapping)	Atom% of M-OOH (based on O atom%)
O	12.82	-
P	21.6	-
Fe	0.52	1.04
Mn	0.01	0.02
Ni	65.04	**11.76**

Table S3. OER performance of different catalysts.

Catalysts	Overpotential in 1.0 M KOH (mV)	
	10 mA cm^{-2}	200 mA cm^{-2}
RuO_2	246	347
Ni_2P	231	389
Ni_2P-ECO	240	379
(Fe) Ni_2P-ECO	212	323
(Mn) Ni_2P-ECO	214	385
(Fe,Mn)Ni_2P-ECO	**207**	**293**

Table S4. The Tafel slopes of catalysts.

Catalysts	Tafel (mv dec^{-1})
NF	175
Ni_2P	114
Ni_2P-ECO	108
(Fe) Ni_2P-ECO	80
(Mn) Ni_2P-ECO	113
(Fe,Mn)Ni_2P-ECO	**64**

Table S5. The Cdl and ECSA of different catalysts.

Catalysts	C_{dl} (mF cm^{-2})	ECSA (cm^{-2})
NF	1.7	43.5
Ni_2P	2.9	73.0
Ni_2P-ECO	2.7	67.9
(Fe) Ni_2P-ECO	4..8	118.6
(Mn) Ni_2P-ECO	3.1	77.6
(Fe,Mn)Ni_2P-ECO	3.2	79.7

Table S6. Gas chromatographic peak area of O_2 and N_2 in electrolyzer before and after electrolysis.

	O_2	N_2	O_2/N_2
Air	846768.3	2509930.2-	0.337
After 0 s	59129.1	180840.9	0.327
After 7200 s	193334.2	319348.8	0.605

Table S7. Comparison of (Fe,Mn)Ni_2P-ECO catalyst with reported OER catalysts in 1.0 M KOH.

Electrolyte	Catalysts	Overpotential at 10 mA cm^{-2} (mV)	FE (%)	Ref.
1.0 M KOH	(Fe,Mn)Ni_2P-ECO	**207**	99.8	This work
	$MnGa_4$/NF	291	97	1
	Ni-Fe-Se	249	-	2
	Co-Fe-W	300	≈100	3
	Co-Cu-Fe-Mo (oxy)hydroxide	199	-	4
	EO-$InNNi_3$	410	-	5
	Ir/CoNiB	178	99	6
	$FeNi(OH)_x$@NF	198	97.4	7
	NiFe-LDH	230		8
	V-Ni_2P/NF-AC	221	98.6±1.5	9
	NiFeCr/NF	270	-	10
	Mn-CoP	261	99	11
	(Mn,Fe)/Ni/Co oxides	363	-	12
	$Fe_{0.3}Ni_{0.7}O_x$/MWCNTS-O_x	320	-	13
	CoMnP	330	96	14
	Ni-Mn-FeP	250	97.3	15
	NiFe-LDH NSs	300	≈100	16
	$FeSe_2$	330	≈100	17

3. References

[1] P. Menezes, C. Walter, J. Hausmann, R. Suito, C. Schlesiger, S. Praetz, V. Yu, Verchenko, A. Shevelkov, M. Driess, *Angew. Chem. Int. Ed.,* 2019, **58**, 16569−16574.

[2] Z. Wu, H. Zhang, S. Zuo, Y. Wang, S. Zhang, J. Zhang, S. Zang, X. Wen, *Adv. Mater.,* 2021, **33**, 2103004.

[3] J. Chen, H. Li, Z. Yu, C. Liu, Z. Yuan, C. Wang, S. Zhao, G. Henkelman, S. Li, L. Wei, Y. Chen, Adv. *Energy Mater.,* 2020, **10**, 2002593.

[4] L. Zhang, W. Cai, N. Bao, *Adv. Mater.,* 2021, **33**, 2100745.

[5] S. She, Y. Zhu, H. Tahini, X. Wu, D. Guan, Y. Chen, J. Dai, Y. Chen, W. Tang, S. Smith, H. Wang, W. Zhu, Z. Shao, *Small,* 2020, **16**, 2006800.

[6] C. Wang, P. Zhai, M. Xia, Y. Wu, B. Zhang, Z. Li, L. Ran, J. Gao, X. Zhang, Z. Fan, L. Sun, J. Hou, *Angew. Chem. Int. Ed.,* 2021, **60**, 27126−27134.

[7] B. Li, J. Zhao, Y. Wu, G. Zhang, H. Wu, F. Lyu, J. He, J. Fan, J. Lu, Y. Li, *Small,* 2023, 2301715.

[8] Y. Wu, J. Yang, T. Tu, W. Li, P. Zhang, Y. Zhou, J. Li, J. Li, S. Sun, *Angew. Chem. Int. Ed.,* 2021, **60**, 26829−26836.

[9] T. Zhao, X. Shen, Y. Wang, R. Hocking, Y. Li, C. Rong, K. Dastafkan, Z. Sun, C. Zhao, *Adv. Funct. Mater.,* 2021, **31**, 2100614.

[10] X. Bo, R. Hocking, S. Zhou, Y. Li, X. Chen, J. Zhuang, Y. Du, C. Zhao, *Energy Environ. Sci.,* 2020, **13**, 4225−4237.

[11] M. Wang, W. Fu, L. Du, Y. Wei, P. Rao, L. Wei, X. Zhao, Y. Wang, S. Sun, *Appl. Surf. Sci.,* 2020, **515**, 146059.

[12] T. Priamushko, P. Guggenberger, A. Mautner, J. Lee, R. Ryoo, F. Kleitz, *ACS Appl. Energy Mater.,* 2022, **5**, 13385−13397.

[13] D. Morales, M. Kazakova, S. Dieckhöfer, A. Selyutin, G. Golubtsov, W. Schuhmann, J. Masa, *Adv. Funct. Mater.,* 2020, **30**, 1905992.

[14] D. Li, H. Baydoun, C. Verani, S. Brock, *J. Am. Chem. Soc.,* 2016, **138**, 4006−4009.

[15] Y. Liu, Z. Zhang, L. Zhang, Y. Xia, H. Wang, H. Liu, S. Ge, J. Yu, *J. Mater. Chem. A,* 2022, **10**, 22125.

[16] R. Gao, D. Yan, *Nano Research,* 2018, **11**, 1883−1894.

[17] R. Gao, H. Zhang, D. Yan, *Nano Energy,* 2017, **31**, 90−95.

[18] G. Kresse, J. Furthmüller, *Comp. Mater. Sci.,* 1996, **6**, 15−50.

[19] G. Kresse, J. Furthmüller, *Phys. Rev. B.,* 1996, **54**, 11169−11186.

[20] J. Perdew, K. Burke, M. Ernzerhof, *Phys. Rev. Lett.,* 1996, **77**, 3865−3868.

[21] S. Grimme, *J. Comput. Chem.,* 2006, **27**, 1787−1799.

[22] R. Luo, Y. Li, L. Xing, N. Wang, R. Zhong, Z. Qian, C. Du, G. Yin, Y. Wang, L. Du, *Appl. Catal. B: Environ.,* 2022, **311**, 121357.

[23] Q. Zhang, M. Sun, M. Yao, J. Zhu, S. Yang, L. Chen, B. Sun, J. Zhang, W. Hu, P. Zhao, *J. Colloid Interf. Sci.,* 2022, **623**, 617−626.

[24] M. Mota, M. Bajdich, V. Viswanathan, A. Vojvodic, A. Bell, *J. Nørskov, J. Phys. Chem. C,* 2012, **116**, 21077−21082.

[25] M. Liu, Z. Sun, C. Zhang, S. Li, C. He, Y. Liu, Z. Zhao, *J. Mater. Chem. A.,* 2022, **10,** 13410.